

NASA/TM—2012-217704

AIAA-2012-3129



# Mechanism of Water Droplet Breakup Near the Leading Edge of an Airfoil

*Mario Vargas*  
*Glenn Research Center, Cleveland, Ohio*

*Suthyvann Sor and Adelaida Garcia Magarino*  
*Instituto Nacional de Tecnica Aeroespacial, Madrid, Spain*

## NASA STI Program . . . in Profile

Since its founding, NASA has been dedicated to the advancement of aeronautics and space science. The NASA Scientific and Technical Information (STI) program plays a key part in helping NASA maintain this important role.

The NASA STI Program operates under the auspices of the Agency Chief Information Officer. It collects, organizes, provides for archiving, and disseminates NASA's STI. The NASA STI program provides access to the NASA Aeronautics and Space Database and its public interface, the NASA Technical Reports Server, thus providing one of the largest collections of aeronautical and space science STI in the world. Results are published in both non-NASA channels and by NASA in the NASA STI Report Series, which includes the following report types:

- **TECHNICAL PUBLICATION.** Reports of completed research or a major significant phase of research that present the results of NASA programs and include extensive data or theoretical analysis. Includes compilations of significant scientific and technical data and information deemed to be of continuing reference value. NASA counterpart of peer-reviewed formal professional papers but has less stringent limitations on manuscript length and extent of graphic presentations.
- **TECHNICAL MEMORANDUM.** Scientific and technical findings that are preliminary or of specialized interest, e.g., quick release reports, working papers, and bibliographies that contain minimal annotation. Does not contain extensive analysis.
- **CONTRACTOR REPORT.** Scientific and technical findings by NASA-sponsored contractors and grantees.

- **CONFERENCE PUBLICATION.** Collected papers from scientific and technical conferences, symposia, seminars, or other meetings sponsored or cosponsored by NASA.
- **SPECIAL PUBLICATION.** Scientific, technical, or historical information from NASA programs, projects, and missions, often concerned with subjects having substantial public interest.
- **TECHNICAL TRANSLATION.** English-language translations of foreign scientific and technical material pertinent to NASA's mission.

Specialized services also include creating custom thesauri, building customized databases, organizing and publishing research results.

For more information about the NASA STI program, see the following:

- Access the NASA STI program home page at <http://www.sti.nasa.gov>
- E-mail your question to [help@sti.nasa.gov](mailto:help@sti.nasa.gov)
- Fax your question to the NASA STI Information Desk at 443-757-5803
- Phone the NASA STI Information Desk at 443-757-5802
- Write to:  
STI Information Desk  
NASA Center for AeroSpace Information  
7115 Standard Drive  
Hanover, MD 21076-1320



# Mechanism of Water Droplet Breakup Near the Leading Edge of an Airfoil

*Mario Vargas*  
*Glenn Research Center, Cleveland, Ohio*

*Suthyvann Sor and Adelaida Garcia Magarino*  
*Instituto Nacional de Tecnica Aeroespacial, Madrid, Spain*

Prepared for the  
Atmospheric Space Environments Conference  
sponsored by the American Institute of Aeronautics and Astronautics  
New Orleans, Louisiana, June 25–28, 2012

National Aeronautics and  
Space Administration

Glenn Research Center  
Cleveland, Ohio 44135

## Acknowledgments

The authors would like to thank Mr. Chris Lynch for his excellent imaging work during the experiment. Thanks to Dr. Alex Feo, Dr. Mark Potapczuk, and Dr. Peter Struk for reviewing the paper, and to Dr. Andy Broeren for his help with the monosize droplet generator during the pre-test imaging work done at the NASA Icing Branch Flow Laboratory. Thanks also to Mr. Yago Sanchez and Mr. Carlos Molina from ALAVA INGENIEROS for their support and expertise during the experiment. Thanks to all rotating rig INTA personnel for their excellent support in the preparation work and during the execution of the test program. The present work is part of the NASA/INTA collaboration under a Space Act Agreement. It is funded by the Atmospheric Environment Safety Technologies (AEST) Project, Aviation Safety Program (AvSP). Special thanks to Dr. Ron Colantonio for his support of the effort.

Trade names and trademarks are used in this report for identification only. Their usage does not constitute an official endorsement, either expressed or implied, by the National Aeronautics and Space Administration.

*Level of Review:* This material has been technically reviewed by technical management.

Available from

NASA Center for Aerospace Information  
7115 Standard Drive  
Hanover, MD 21076-1320

National Technical Information Service  
5301 Shawnee Road  
Alexandria, VA 22312

Available electronically at <http://www.sti.nasa.gov>

# Mechanism of Water Droplet Breakup Near the Leading Edge of an Airfoil

Mario Vargas  
National Aeronautics and Space Administration  
Glenn Research Center  
Brook Park, Ohio 44135

Suthyvann Sor and Adelaida Garcia Magarino  
Instituto Nacional de Técnica Aeroespacial  
Madrid, Spain

## Abstract

This work presents results of an experimental study on droplet deformation and breakup near the leading edge of an airfoil. The experiment was conducted in the rotating rig test cell at the Instituto Nacional de Técnica Aeroespacial (INTA) in Madrid, Spain. The airfoil model was placed at the end of the rotating arm and a monosize droplet generator produced droplets that fell from above, perpendicular to the path of the airfoil. The interaction between the droplets and the airfoil was captured with high speed imaging and allowed observation of droplet deformation and breakup as the droplet approached the airfoil near the stagnation line. Image processing software was used to measure the position of the droplet centroid, equivalent diameter, perimeter, area, and the major and minor axes of an ellipse superimposed over the deforming droplet. The horizontal and vertical displacement of each droplet against time was also measured, and the velocity, acceleration, Weber number, Bond number, Reynolds number, and the drag coefficients were calculated along the path of the droplet to the beginning of breakup. Droplet deformation is defined and studied against main parameters. The high speed imaging allowed observation of the actual mechanism of breakup and identification of the sequence of configurations from the initiation of the breakup to the disintegration of the droplet. Results and comparisons are presented for droplets of diameters in the range of 500 to 1800  $\mu\text{m}$ , and airfoil velocities of 70 and 90 m/sec.

## Nomenclature

avi	Audio video interleave movie format
Bo	Bond number
$c$	Airfoil chord
$C_d$	Drag coefficient
$D$	Droplet diameter
DBKUP	Airfoil designation
$f$	Square wave frequency introduced by activating a piezoelectric transducer
INTA	Instituto Nacional de Técnica Aeroespacial
LED	Light Emitting Diode
PIV	Particle Image Velocimetry
$Q$	Water flow rate
Re	Reynolds number
SLD	Supercooled Large Droplets
$V$	Velocity
$V_{\text{slip}}$	Slip Velocity, relative velocity between the droplet and the air: ( $\mathbf{V}_{\text{droplet}} - \mathbf{V}_{\text{air}}$ )
We	Weber number

## Introduction

Supercooled Large Droplet (SLD) breakup near the leading edge of large transport airfoils may alter the mass flux of water reaching the leading edge and be a factor that needs to be accounted for in the prediction of ice accretion formation in icing codes. Studies of droplet breakup can provide experimental data on the main parameters of droplet deformation and the sequence of steps that lead to droplet disintegration. They can indicate the location where droplet breakup is initiated and the size and shape of the pieces that may be carried away by the airflow as the droplet goes through the breakup process and disintegrates or impacts the surface of the airfoil. They can also provide an understanding of the physics involved in the process of deformation and breakup.

Previous studies (Refs. 1 and 2) measured the droplet horizontal and vertical displacement against time and calculated the velocity, acceleration, Weber number, Bond number, and Reynolds number along the path of the droplet as it approached the leading edge near the stagnation line. The studies also presented the sequence of droplet deformation that leads to the initiation of breakup. Those studies were carried out for an airfoil with a chord of 0.47 m and droplet diameters up to 500  $\mu\text{m}$  and allowed defining the beginning of the actual droplet breakup as the point along the path at which the thickness of the droplet reaches a minimum. The final sequence of the droplet breakup was observed but not all the details were captured. The studies indicated the need to continue the study of droplet deformation, to do a detailed observation of the droplet breakup from its initiation to total disintegration, to extend the testing to airfoils of different chord size and to increase the size of the droplets up to 1800  $\mu\text{m}$ .

This paper provides the results of a droplet deformation and breakup experiment conducted in July of 2011 in the rotating rig test cell at the Instituto Nacional de Técnica Aeroespacial (INTA) in Madrid, Spain. The experiment is part of an international agreement between NASA and INTA. The experiment was conducted on airfoils with chord lengths of 0.21, 0.47, and 0.71 m placed at the end of an arm rotating about a central axis at speeds from 50 to 90 m/sec. A monosize droplet generator was employed to produce droplets from 100 to 1800  $\mu\text{m}$  that were allowed to fall from above, perpendicular to the path of the model airfoil at a given location. A high speed imaging system was used to capture the droplet deformation and breakup as the droplets approached the leading edge of the airfoil along the stagnation line (Figs. 1 and 2).

The overall objective of the experiment was to extend previous experimental results on droplet deformation to three airfoils of same geometry but different chord size, to increase the range of droplet diameters tested, and to obtain a more detailed observation of the actual mechanism of droplet deformation and breakup from its initiation to disintegration. For a given droplet, digital imaging processing was employed to measure the diameter, coordinates of the centroid, the area, the perimeter and the horizontal and vertical dimensions at each location of a droplet along its path. The droplet displacement against time was measured and the important parameters along the drop path were calculated. The high speed movies allowed observing the details of the droplet breakup sequence. The image processing data and the calculated parameters were used to study the droplet deformation.

The present work is a continuation and extension of previous research efforts to measure the important parameters involved in droplet deformation and breakup, to study the effect of airfoil size and to identify the mechanism of droplet breakup as droplets approach the leading edge of an airfoil along the stagnation line. The results will help in determining if icing codes need to be modified to account for droplet breakup when the size of the droplets is in the SLD regime.

## Experimental Setup

The experimental setup has four main elements: the rotating arm unit, the airfoil attached at the end of the arm, the monosize droplet generator and the high speed imaging system. Figure 1 shows the conceptual view of the experiment setup with all the elements except the high speed imaging system. Figure 2 shows the experimental setup components in the test cell before a run. The setup was identical to the one used in previous experiments (Refs. 1 and 2).

## A. Rotating Arm Unit

The rotating arm unit consists of a 5 kW electric motor mounted on a support structure that rests on a solid base attached to the floor (Fig. 2). The support structure is attached to the base through four slip ring vibration dampers. The motor is placed inside the support structure with the axle perpendicular to the horizontal plane and in the direction of the ceiling. A rotating arm is attached to the axle of the motor.

The length of the arm measured from the center of the axle to the airfoil model attached at the end is 2.37 m (93.3 in.). For balancing, vibration control and additional strength, a system of struts is mounted on the axle and opposite the arm location (Fig. 2). Accelerometers on the arm and the axle are used to monitor the arm vibrations. The revolutions per minute of the arm are measured using a light emitting diode (LED) optical system. The LED is mounted on the supporting structure with its beam pointed at an angle toward the rotating axle. A small reflecting tape mounted on the rotating axle reflects the light in each revolution. The reflected light is picked up by a detector placed next to the LED. Each time that the detector registers the reflected light from the LED one revolution of the arm is counted. The control of the electric motor is located in the control room, a section of the test cell separated from the rotating rig by a safety glass window (Fig. 2). The revolutions per minute of the arm can be adjusted to set the airfoil model at velocities from 0 to 90 m/sec at less than 1 m/sec intervals.

## B. Airfoil Models

Three airfoils were used during the experiment. They have the same geometry but different chord size. They are a generic type of thick airfoil designated as DBKUP 001, DBKUP 002, and DBKUP 003 (Fig. 3). Table 1 lists the coordinates of the airfoil. This type of airfoil geometry was chosen for the experiment because it is a blunt shape that simulates a scaled version of the type of leading edge shape found on large transport airfoils. The chord sizes of the airfoils are 0.21 m (8.3 in.), 0.47 m (18.5 in.) and 0.71 m (30.0 in.), respectively. The airfoil geometry was the same as that used in previous experiments (Ref. 1).

## C. Monosize Droplet Generator

A TSI MDG-100 Monosize Droplet Generator is used to produce water droplets within a diameter range from 100 to 500  $\mu\text{m}$ . The droplet generator (Figs. 2 and 3) consists of a distilled water container, an electric pump, a power supply to drive the electric pump, a flow control valve, a frequency generator and the vibration head. The electric water pump delivers the water flow from the container to the vibration head. The high precision flow rate control valve with a manometer allows fine adjustment of the flow rate before the water reaches the vibration head. At the vibration head the water is forced through a small orifice (100  $\mu\text{m}$  in diameter) and a jet is formed. A disturbance in the form of a square wave at the appropriate frequency is introduced by activating a piezoelectric transducer controlled with a BK Precision model 4011A frequency generator. The jet is unstable at resonant frequencies and breaks into uniform droplets. For a given orifice diameter, flow rate and excitation frequency the diameter of the generated droplets is given by the equation:

$$D(\mu\text{m}) = 317 \left[ \frac{Q(\text{cc/min})}{f(\text{kHz})} \right]^{1/3} \quad (1)$$

where  $Q$  is the water flow rate in cubic centimeters per minute;  $f$  is the frequency in kilohertz; and  $D$  is the diameter of the droplets in  $\mu\text{m}$ . Prior to the droplet breakup high speed test, the monosize droplet generator was calibrated for orifices from 100 to 800  $\mu\text{m}$ . The TSI MDG-100 Monosize Droplet Generator was not originally designed for orifice sizes larger than 100  $\mu\text{m}$  but when tested with commercially available larger orifices it performed well and droplets sizes up to 1500  $\mu\text{m}$  could be generated.

## **D. High Speed Imaging System**

The high speed imaging system consists of the high speed camera (Fig. 2), the camera software, the lens system and the lighting. The high speed camera used during the experiment was a Photron SA-5. The camera can capture images at rates from 1000 to 1,000,000 frames per second (fps). During the experiment frames rates of 50000, 75000, and 150000 fps were used with corresponding resolutions given in pixels for the horizontal and vertical directions: 192×512, 192×312, and 128×184. As the frame rate is increased, the resolution of the camera decreases. The camera has a maximum shutter speed of 1 (μs) at frames rates below 775,000 fps. The camera software employed for capturing the high speed image sequences is Photron's FASTCAM Viewer (PFV) and is part of the camera system. The same software was used for post-processing the image sequences to generate the data movies for data analysis and to select the frames at which the droplet tracking was to begin and end.

During the experiment one lens configuration was used for two magnifications of the droplet deformation and/or breakup. The lens configuration consisted of a 200 mm Micro Nikkor lens with a 2x doubler added between the camera and the 200 mm lens to double the focal length of the microlens. The two magnifications were achieved by placing the camera at two different distances from the location where the droplets were falling at 0.24 m (9.25 in.) along the span of the airfoil. For the first magnification the distance was 0.91 m (36 in.) and for the second the distance was 0.36 m (14 in.). The lighting was designed to illuminate the droplets from behind to create a shadowgraph (black color of the droplets against a white-gray background). The light source was a 2000 W Xenon light with a lens to focus the beam.

## **Test Procedure and Test Matrix**

### **A. Test Procedure**

Before a test run, the high speed camera system is aligned so that the line of sight of the lens is parallel to the direction along the span of the airfoil at the midpoint of the leading edge (stagnation line along the span). The rotating arm is set at the position where the falling droplets from the monosize droplet generator will just graze the leading edge. The airfoil is held at the same location during the whole alignment process. The camera is placed at the distance required by the optics to obtain the needed magnification and such that the center of the lens depth of field is at the location where the falling droplets graze the airfoil leading edge. The camera sits on a x-y positioning table that allows careful adjustments in either direction. A custom made adaptor, designed to hold a laser pointer so that the laser beam is aligned with the camera lens, is inserted into the camera lens housing. The camera position is adjusted so that the laser beam from the laser pointer is parallel to the span of the airfoil (grazing it). This ensures that the direction of the lens is parallel to the direction of the airfoil span.

The airfoil is moved from the alignment position and a ruler with the smallest subdivision of 1 mm is placed at the location where the droplets will graze the leading edge of the airfoil. The camera is focused on the ruler and the number of pixels per millimeter is recorded, since the number of pixels in the camera sensor and the field of view are known. This conversion is used during the data analysis to measure the droplet diameter. The monosize droplet generator controls are adjusted to produce the range of droplet sizes needed. The personnel withdraw to the control room, where they are able to observe the motion and operation of the rotating arm through a safety glass. The camera is controlled with software run on a laptop computer located in the control room. The software is used to start the camera and set the controlling parameters including frame rate and shutter speed, and allows writing information on each camera frame above the recorded image. The following information is recorded on each frame during the experiment: frame rate, time of recording, image resolution, frame number, lens configuration, date and time, arm velocity and target droplet size.

The rotating arm is set in motion at the rotational speed corresponding to the target velocity. When it reaches the target speed, the camera recording is started and maintained for three or more rotations depending on the amount of data wanted for a particular run. Once the recording is completed the rotating



arm is brought to a stop. The high speed movie is analyzed with the camera software to determine the quality of the recording in each of the three or more passes of the airfoil. If the droplets are in focus, the back light is uniform and the image area covers the horizontal displacement of the droplets, the experiment moves to the next test point and the process is repeated.

## **B. Test Matrix**

The test matrix for the experiment was designed to setup the droplet generator for a chosen theoretical droplet diameter. At each droplet size, test points were set for airfoil velocities of 50, 60, 70, 80, and 90 m per second. Frame rate values employed were 25000, 50000, 65100, 75000, 87000, 100000, and 150000 fps. A speed of 75000 fps was used most frequently because it was a middle point between a frame rate that allowed observation of the droplet breakup and a reasonable resolution of 192×312 pixels. Two camera magnifications were employed during the test. The larger magnification gave more detail but only allowed observation of the droplets over a very small distance. The smaller magnification allowed observation of the droplet over a larger distance, from no interaction with the airfoil, to beginning of deformation, deformation and breakup or impact with the airfoil.

## **Data Analysis and Results**

The high speed camera was employed to observe and record the droplet deformation and breakup as the airfoil approached the location of the droplet generator. At each condition a high speed movie of the interaction between the airfoil and the falling droplets was obtained for three or more passes of the airfoil. The movie was recorded in raw format and stored on a hard drive for post processing. Before post processing, each movie for a given run was split into “clips”. Each “clip” consisted of the movie for one pass of the airfoil. A total of 154 runs were conducted and the imaging data were split into 1128 movie clips. In each clip there is usually one or more droplets deforming and/or breaking up. A subset of the data was analyzed and is presented in this paper.

### **A. Data Post Processing**

The camera software was used to generate the clips and to change them from raw format to avi. The change in format from raw to avi was done without using any compression to avoid altering the data. To post process the droplet data from the clips, a data analysis program was developed (Ref. 3). The program has a digital image processing part and a calculation part. It reads the movie in avi format and converts each frame from grayscale to binary for image segmentation and tracking. The program is initialized with the following input: file name of the video clip, camera resolution, frame rate of the movie, chord length of the airfoil tested, assigned number of the droplet being tracked, frame number where the tracking begins and frame number where the tracking ends.

The frame numbers where the tracking begins and ends are selected from the movie clip with help of the camera software. The assigned number of the tracked droplet is obtained from the frame where the tracking begins. The program identifies the droplets in a given frame by numbering them from left to right. In each frame the digital image processing part of the program calculates and/or records the following parameters for the droplet being tracked: frame number, time with respect to the tracking frame, time with respect to the first frame of the movie, x coordinate of the centroid, y coordinate of the centroid, area, perimeter, major and minor axes of an ellipse superimposed on the droplet, equivalent diameter based on the measured area, equivalent diameter based on the volume for an oblate spheroid using the major and minor axes of the superimposed ellipse and calculated assuming the droplet is an oblate spheroid asymmetric about the major axis on the plane of observation, symmetric about the minor axis on the plane of observation and rotationally symmetric about the axis pointing in the direction that the droplet is moving toward the airfoil (Ref. 4).

The diameter based in the volume of the oblate spheroid was used in all calculations. As long as the droplet remains an oblate spheroid with the symmetries mentioned above, this diameter should remain constant since the volume of the droplet does not change (Fig. 4). The diameter based on the area of the droplet cross section varies since the area is the cross section of a three-dimensional body changing in shape. In all the calculations presented in this paper that involve the diameter of the droplet, the diameter used was the one based on the volume of the oblate spheroid (Ref. 4):

$$d = \sqrt{b^2 \cdot a} \quad (2)$$

where  $b$  is the height of the droplet and  $a$  the width.

The calculation part of the program uses the parameters measured in the image processing part to calculate the following parameters with respect to time: horizontal and vertical displacement, velocity of the droplet with respect to the airfoil (frame of reference at rest with respect to the airfoil with the origin at the stagnation point), position of the droplet with respect to the airfoil, slip velocity, acceleration, Weber number, Reynolds number, Bond number and the drag coefficient. For the calculation of the slip velocity at a given location, the velocity of the air at that location is needed. The value of the velocity at a given location with respect to the airfoil and along the stagnation line was obtained using a correlation for air velocity from Particle Image Velocimetry (PIV) measurements conducted in the test cell (Ref. 5) for each of the three airfoil geometries tested.

A droplet is a three-dimensional object. The tracking and measurements are made on a two-dimensional profile of the droplet. In some instances this does not affect the data and conclusions. In other instances the three dimensionality of the droplet is important and will affect the results. If this is the case for the data presented, the effect of the droplet three-dimensionality on the results will be stated and explained.

## B. Data from Digital Image Processing

The digital image processing part of the program allows study of the droplet deformation against time. Data from Run 072011.14C droplet #1 is presented in Figures 5 to 10. The size of the droplet is 1062  $\mu\text{m}$ , the chord of the airfoil is 0.710 m and the velocity of the airfoil is 90 m/sec. The movie clip has a single droplet that was tracked from frame 20 to frame 210. The droplet is initially nearly spherical (Fig. 5(a)) and as it approaches the airfoil it deforms into an asymmetric oblate spheroid (Fig. 5(b)) with a slight forward inclination with respect to the vertical axis. The inclination is small but noticeable. In describing the oblate spheroid, the two axes of the spheroid will be treated as being approximately in the direction of the horizontal and vertical axis. The oblate spheroid is asymmetric about the vertical axis, symmetric about the horizontal axis in the plane of observation, and assumed rotationally symmetric about the axis pointing in the direction of motion (horizontal axis). The front part of the spheroid is initially rounded but slowly becomes flatter as the droplet approaches the airfoil. The process continues until the droplet no longer can sustain the stretching shape against the aerodynamic forces and begins the actual breakup process. The breakup process is discussed in detail in section F.

Figure 6 shows the horizontal displacement of the droplet against time with respect to a frame of reference at rest with respect to the test cell. It is a plot of the centroid x-coordinate against time. The displacement of the droplet increases exponentially. This can be explained as follows, in a frame of reference at rest with respect to the test cell: as the airfoil approaches the droplet, the velocity of the air increases exponentially around the droplet. The droplet is dragged in that direction but its inertia prevents it from following the air velocity and a difference between the velocity of the air and the velocity of the droplet develops (slip velocity) that displaces the droplet and generates aerodynamic forces that deform it. This process can also be explained from a frame of reference at rest with respect to the airfoil. In this frame of reference, when the droplet is far from the airfoil, the droplet approaches the airfoil at the same velocity as the velocity of the air at that location. As the droplet gets closer to the airfoil, a difference between the velocity of the air and the droplet develops (slip velocity) because the air velocity decreases

exponentially along the stagnation line (reaching zero at the stagnation point of the airfoil) and the inertia of the droplet prevents it from following the velocity of the air. The slip velocity increases as the velocity of the air decreases and the generated aerodynamic forces deform the droplet. It is the exponential decrease in the velocity that is reflected in the exponential horizontal displacement of the droplet against time. Since the velocity of the droplet at each time is the tangent to the curve, it will also show an exponential behavior as will the acceleration of the droplet against time. The exponential behavior of the velocity and acceleration propagates to the Weber, Reynolds, and Bond numbers.

Figure 7 shows the vertical displacement of the droplet against time. It is a plot of the centroid y-coordinate against time. It increases linearly with time indicating a constant velocity for the droplet. The reason for the constant velocity is that the droplets are tracked close to the head of the droplet generator where the droplets are ejected at a constant velocity, 2 m/sec for the droplet data presented in Figure 7.

Figure 4 shows the two diameters that were calculated against time. The data in blue (triangles) corresponds to the diameter of a circular surface with the same area as the area of the tracked droplet measured by the program. The program measures the area in pixels. The diameter is measured initially in pixels and converted to micrometers using the resolution value of 14.26 pixels per millimeter used during the whole experiment. The behavior of the diameter against time reflects the change in the area of the tracked droplet as it deforms. If the initial shape of the droplet is close to being spherical, the value of the diameter using a circular cross section gives a good approximation to the real value of the diameter of the three-dimensional spherical droplet. As the droplet deforms and changes its shape, because it is a three-dimensional body the value of the cross sectional area does not remain constant and should not be used to calculate the diameter. However, the volume remains constant as the droplet deforms (assuming density remains constant) and can be used to calculate an equivalent diameter as long as the droplet shape corresponds to an oblate spheroid asymmetric with respect to the vertical axis, symmetric with respect to the horizontal axis and rotationally symmetric with respect to the axis along which it is moving towards the airfoil. The diameter based on the volume of the oblate spheroid is the red data (rectangles) presented in Figure 4. The diameter remains constant along the path providing indirect confirmation that the spheroid is rotationally symmetric about the horizontal axis and giving a more accurate measurement of the diameter needed for calculations. The digital imaging program uses the diameter based on the volume of the spheroid in all the calculations where the diameter is involved. During the final stages of the droplet trajectory, either the shape is departing from an oblate spheroid or the volume is changing somehow. Figure 4 suggests that the shape changes from an oblate spheroid somewhere between 1500 and 2375  $\mu\text{sec}$  and then departs dramatically after 2375  $\mu\text{sec}$ .

Figures 8 and 9 show the minor and major axes of an ellipse superimposed on the deformed droplet against time. The angle of the ellipse (major axis of the ellipse with respect to horizontal axis) is not always  $90^\circ$ . It depends on the specific shape of the droplet that is being superimposed with the ellipse. The width of the droplet (when deforming) is taken as the value of the minor axis, while the height is taken as the value of the major axis of the ellipse. Figure 8 shows how the width of the droplet decreases with time to a minimum and then starts increasing while Figure 9 shows how the height increases at the same time. The moment at which the width of the droplet reaches a minimum is defined as the beginning of the actual “breakup”. Previous to that point the droplet is by definition designated as “deforming”. The point at which the droplet width reaches its minimum value correlates with the time in an image sequence when the droplet no longer continues to stretch and begins moving away from an oblate spheroid shape (Fig. 5(f)). From the beginning of deformation to the point where the actual droplet breakup begins (minimum width), the droplet resembles an oblate spheroid, initially symmetric, then asymmetric with respect to the vertical axis. Up to this point the droplet is deforming. Once the minimum width is reached, the droplet shape begins to deviate from an oblate spheroid and the droplet breakup sequence begins. The height of the droplet tends to follow the opposite pattern: increasing during deformation of the droplet and decreasing during breakup.

The data presented in Figures 4 to 9 is only for one droplet case. In general, the droplet cases analyzed for an airfoil with a 0.710 m chord moving at 90 m/sec follow the same pattern. Differences occur with very large droplets ( $>1200 \mu\text{m}$ ) because they oscillate when falling and change shape during

longer times before the presence of the airfoil is felt and the typical pattern of deformation begins. In those cases, the deformation of the droplet departs from the typical case presented in Figures 4 to 9. Smaller droplets (<500  $\mu\text{m}$ ) have larger surface tension forces and have greater resistance to the pull of the aerodynamic forces toward deformation and breakup. They deform less and exhibit only part of the typical deformation pattern.

### **C. Calculated Data**

Once the horizontal displacement of the droplet is measured at each location along the path, the important parameters can be calculated: velocity, acceleration, slip velocity, Weber number, Reynolds number, Bond number, and drag coefficient. The calculation of these parameters has been presented in previous publications (Refs. 1 and 2). The same droplet data case used in section B, Run 072011.14C droplet #1, will be used in this section.

Figure 10 shows the slip velocity, the air velocity and the droplet velocity against the distance along the stagnation line from the leading edge of the airfoil. The exponential behavior of the slip velocity is expected since the slip velocity is the difference between the velocity of the air and the velocity of the droplet as seen in a frame of reference at rest with respect to the airfoil. As the air velocity decreases exponentially toward zero at the stagnation point, a difference in the velocity of the air and the droplet (slip velocity) develops due to the inertia of the droplet, and aerodynamic forces produce drag on the droplet decelerating it and deforming it. The slip velocity increases all along the trajectory due to the continued exponential decrease of the air velocity. Since the slip velocity increases exponentially, the Weber number (which is proportional to the square of the slip velocity) and the Reynolds number (which is proportional to the slip velocity) will follow the same behavior. Figures 11 and 12 show the Weber number and the Reynolds numbers against the distance along the stagnation line from the leading edge of the airfoil. The same behavior is noticed for the acceleration of the droplet and the Bond number since the acceleration is the second derivative of the function representing displacement against time.

The exponential increase in the Weber number has special significance since it is the ratio of the aerodynamic forces trying to deform the droplet against the surface tension forces opposing them and trying to hold the droplet together. As the Weber number increases exponentially, the droplet is subject to higher and higher forces that deform it and in some cases break it apart. Although the forces increase exponentially, the increase is gradual allowing the droplet to slowly deform over time and tolerate relatively high Weber numbers before beginning to break up. In this sense, studies done in a rotating arm experimental configuration are different from studies done in other configurations where a droplet or droplets are suddenly subject to high Weber numbers. This suggests that the results found here are more representative of breakup for an airfoil encountering droplets suspended in air than the results of experiments with droplets injected into a moving airstream.

### **D. Errors Associated With the Data**

Errors in the data come from three main sources: measurement of the diameter, curve fitting and choice of threshold value during the conversion of images from grayscale to binary. The determination of the diameter from use of the oblate spheroid volume is a larger error than any of these during the final stages of the trajectory. For the example used here, the departure from the oblate spheroid volume after 2375  $\mu\text{m}$  would alter the calculation of the equivalent diameter and thus change the determination of the non-dimensional parameters.

The diameter of the droplets is used to study droplet deformation and to calculate the non-dimensional numbers, so errors in its measurement propagate to the Weber, Reynolds and Bond numbers. The error in its measurement results from limitations in the resolution of the images. The resolution was confined to 14.26 pixels per millimeter due to the imaging setup. The measurement of the diameter in the images has an uncertainty of at least one pixel. For droplets of 500, 1000, and 1500  $\mu\text{m}$  the corresponding

error is 14, 7, and 4.7 percent. For droplets of 250  $\mu\text{m}$  the error grows to 28 percent and becomes even larger for smaller drops. For this reason only droplets with diameters larger than 500  $\mu\text{m}$  were analyzed.

Another source of error that affects the measurement of the slip velocity and the non-dimensional parameters is the curve fitting of the droplet horizontal displacement against time. The values of the velocity (tangent to the curve) and of the acceleration (tangent to the velocity against time curve) are sensitive to the choice of the curve fit for the experimental data. Since the horizontal displacement grows exponentially with time, an exponential curve fit works well. Exponential curve fitting can be done with a function of the form  $y = A_0 \exp[\beta \cdot x]$  or a combination of exponentials  $y = y_0 + a \cdot \exp[bx] + c \cdot \exp[dx] +$

The fit of the curve can be controlled monitoring the statistical parameters but variations in the calculated velocity appear depending on how many exponentials are used and the initial guess used to calculate the coefficients (a, b, c, d,..). The curve fitting for the data presented in this paper was done with two exponentials:  $y = y_0 + a \cdot \exp[bx] + c \cdot \exp[dx]$ .

The choice of the threshold value used for the conversion of grayscale to binary images is an additional source of error. A movie frame in grayscale is a two dimensional array of intensity values between 1 and 255, that were measured in the camera sensor physical pixels. To identify an object and track it from one frame to another, image segmentation needs to be done. To do image segmentation, the image needs to be converted from grayscale to binary. The conversion is done choosing a cutoff value between 1 and 255. This value is called the threshold value. If an element of the image array is above this value, its intensity is converted to 1, if it is below this value its intensity is converted to 0. In this way the two-dimensional array is converted to 0s and 1s, a binary image. The change from grayscale to binary selects the pixels in the movie frame corresponding to an object and, consequently affects the measurement of some parameters of that object such as area and diameter.

There are several methods that can be used to select the threshold value. For the digital imaging part of the data analysis program, Otsu's method (Ref. 7) was used because it is consistent and well founded and is used in many commercially available programs. To evaluate the error of the thresholding method, a limited study was conducted with nineteen droplets. The droplet diameters were measured from their grayscale images using the camera software in a systematic way and compared to the values given by the Otsu method. The measurements were done for only the first tracking frame in each of the nineteen tracking movies. The effect of the threshold value is presented in Figure 13. An error of 13 percent was found in the measurement of the diameter when using the Otsu method, assuming that the values from the grayscale image have minimal error. The Otsu method was used for the binary conversion of grayscale images in all of the data presented in this paper. This error is independent of what happens to the droplets and other errors. It is always present in the image processing part in the conversion from grayscale to binary.

## **E. Droplet Deformation**

The objective of the studies done on droplets approaching the leading edge of the airfoil along the stagnation line is to gain understanding on the physics of the process and to measure droplet deformation and breakup. The first studies (Refs. 1 and 2) focused on an initial understanding of how the droplets behaved as they approached the airfoil and measured the main parameters involved: horizontal displacement, velocity, acceleration, Weber number, Reynolds number, Bond number and drag coefficient. The focus of the present study is on droplet deformation, drag coefficient, and the sequence of the actual droplet breakup. Droplet deformation and drag coefficients will be discussed in this section, and droplet breakup in section F.

As the droplets approach the airfoil and are subjected to the aerodynamic forces generated by the increasing slip velocity, their shape changes from spherical to oblate spheroid. The oblate spheroid is asymmetric with respect to the vertical axis, symmetric with respect to the horizontal axis and assumed rotationally symmetric about the axis pointing in the direction of motion of the droplet. This assumption is based on observations of the images and the similarity in the deformation shape of the droplets of different sizes at different times in their paths. Nevertheless it remains an assumption until we can obtain

front images of the droplets to test its validity. Ideally, in a study of droplet deformation the whole shape of the droplet or the two-dimensional profile would be studied. But in the study of a complex system such as the shape of the droplet it is better to begin with the simplest possible representation of deformation and add complexity later. In this study, the ratio of the height (major axis  $b$  of the superimposed ellipse) of the deforming droplet to its width (minor axis of the superimposed ellipse) was chosen as the parameter to represent deformation.

Droplet deformation =  $b/a$  = major axis of superimposed ellipse/minor axis of superimposed ellipse

To study deformation, a subset of nineteen droplets was selected. The chosen droplets were nearly spherical at the start of tracking, and the diameters were near values of 500, 750, 1000, 1250, 1500 or 1750  $\mu\text{m}$ . Table 2 shows the test conditions for the selected droplets. All of the selected droplets were for a 0.710 m chord airfoil moving at 90 m/sec. Droplets below 500  $\mu\text{m}$  were not selected because of the higher error involved in the measurement of the diameter as discussed in section D.

The deformation against time, slip velocity, Weber number, Reynolds number and Bond numbers was studied. In general the droplet behavior was similar and is illustrated in Figures 14 to 20 for the case of a droplet with a diameter of 1431  $\mu\text{m}$ , Run 072611.15B.9 droplet #2. The deformation increases exponentially with time, the rate of change of the deformation (tangent to the curve) increasing along the whole curve (Fig. 14). The behavior of the deformation against the slip velocity, Reynolds number and Weber number is slightly different. These parameters are changing because they are based upon the slip velocity and the droplet diameter and these are changing. Initially the deformation follows an exponential behavior but then the curve becomes almost linear until droplet breakup begins. Initially the rate of change of the deformation (tangent to the curve) increases but then levels off and remains approximately constant. The deformation against the Weber number ( $We$ ) is presented in Figure 15 and the curves for the slip velocity and the Reynolds number ( $Re$ ) follow the same pattern. A plot of the deformation  $b/a$  against  $We*Re$  accentuates the part of the curve that is more linear but overall was found to be similar to the plot in Figure 15 and for that reason is not presented with the figures. In the case of the deformation against the Bond number (Fig. 16), the rate of change of the deformation decreases initially and then remains nearly constant until the breakup of the droplet begins. Since the slip velocity, the Weber number, the Reynolds number and the Bond number have an exponential behavior against time, it would be expected for the deformation to follow the same pattern. It does to an extent, but is less pronounced and part of the curve is almost linear. This seems to indicate that the shape of the droplet at a given position depends on additional parameters intrinsic to the droplet, for example internal circulation of the water inside the droplet that will create an additional internal pressure at the droplet surface and be another parameter that influences the shape of the droplet.

The change in deformation with droplet diameter at a slip velocity of 60 m/sec is plotted in Figure 17. There is scatter in this data, even for droplets with diameters fairly close to each other and therefore with similar Weber and Reynolds numbers. The scatter in the data for droplets with the similar Weber and Reynolds numbers indicates that other parameters are important in the droplet deformation. In particular, if the droplets are subject to different accelerations, droplets of the same diameter have different deformation. In Figure 18(a) the Bond number is plotted against the diameter for the same droplets analyzed in Figure 17. For droplets with similar Bond number values, going back to Figure 17, it can be observed that there is minimal scatter. For droplets with different Bond numbers and in some cases very close values of the diameter, the data for those droplets shows scatter in Figure 17. In Figure 18(b) the deformation ( $b/a$ ) scaled by the Bond number is plotted against droplet diameter. The scattering is less pronounced. The standard deviation for the data in Figures 17 is 1.34 while for the data in Figure 18(b) it is 0.4. Thus droplet deformation depends on several parameters: Weber number, Reynolds number, Bond number and possibly others, complicating comparisons between droplets. The plots of deformation versus diameter for slip velocities of 25 to 70 m/sec at 5 m/sec intervals are similar: less scattering of the data at the lower slip velocities, increasing as the slip velocity increases.

As the droplet deforms, the flow field around the droplet changes and the drag that causes the deceleration of the droplet changes. The drag coefficient would be expected to increase monotonically with the deformation since the shape of the droplet changes to an asymmetric oblate spheroid of increasingly flatter and flatter shape (for example a disk exhibits higher drag coefficients than a solid sphere). In Figure 19 the drag coefficient for a droplet with a diameter of 1431  $\mu\text{m}$ , Run 072611.15B.9 droplet #2, is plotted against deformation until droplet breakup begins. As expected the drag coefficient increases linearly with the deformation. In Figure 20 the drag coefficient is plotted against the Reynolds number. In the same plot the drag coefficient for a solid sphere is plotted for comparison. While the drag for a solid sphere remains at a value of 0.4 in the Reynolds number range of 2000 to 8000, the droplet drag coefficient initially is also 0.4 when the droplet is still spherical but then increases linearly as the droplet deforms from a sphere to an asymmetric spheroid flatter and flatter as the deformation ( $b/a$ ) increases.

## F. Droplet Breakup

Droplet breakup begins when the value of the minor axis of the superimposed ellipse (width of the droplet) reaches a minimum. Up to this point the droplet has passed from a spherical shape to a non-symmetric oblate spheroid. In this process the width of the droplet decreases as the oblate spheroid stretches in height and reaches a point where its shape begins to deviate from an oblate spheroid and no longer can sustain the air flow pressure and viscous forces and begins the process that will lead to the droplet disintegration.

Analysis of the imaging data indicates that in all the cases where the droplets are larger than 500  $\mu\text{m}$ , the sequence of droplet breakup is similar and can be separated in distinct stages. Without a detailed knowledge of the forces acting on the droplet at the different stages of its breakup these observations are qualitative only. The imaging data does give a clear view of how the process occurs and its different stages. Figure 21 shows the sequence of a droplet breaking up beginning at the point where the droplet width has decreased to a minimum but is still showing the shape of an asymmetric oblate spheroid flattened in the front part and quite elongated (Fig. 21(a)). At the initiation of the breakup the droplet shape changes, the front flat part starts to develop a bulge while the back area becomes flatter (Figs. 21(b), (c)). The bulge at the front develops into what from the side looks like a “hat” shape (Fig. 21(d)). This shape continues to increase in size (Figs. 21(e), (f), (g)), then starts shearing at the sides (Fig. 21(h)) and continues to shear losing mass in the process (Figs. 21 (i), (j)) until it hits the airfoil or all the mass is lost.

The images are a two-dimensional view of a three-dimensional process of droplet disintegration, but they convey the three dimensionality of the process and the first indication that there is rotational symmetry around the axis pointing in the direction of the motion of the droplet. Additional color images were taken of the droplet breakup process that give better views of the three dimensionality of the droplet breaking up and the loss of mass by shearing. Figure 22 shows droplets in the last stage of breakup. Part of the core of the original droplet is still visible and losing water by shearing. It is followed by a trail of the water that ends in a cloud of smaller droplets. During breakup the droplet initially has a radical change from an oblate spheroid to a “hat” shape and then begins losing its mass by a shearing process. This mass loss is in the form of a tail that trails the droplet and ends in a cloud of smaller droplets. There is a definite time scale for the process, determined by the shearing mechanism that causes the disintegration of the droplet. For the droplet breakup presented in Figure 21 is of the order of 120  $\mu\text{m}$ .

## G. Distance From Airfoil Leading Edge at Which Droplets Begin Breakup

The distance at which the droplet begins its breakup (minimum value of the width of the droplet) was measured for droplets of different sizes for the 0.710 and 0.470 m chord-size airfoil models. The resultant data was completely scattered. Comparing the distance at which droplets begin breakup is not correct unless the droplets share the same history with respect to the parameters that determine their deformation and

breakup. The only statement that can be made about the data is that for both airfoils all of the droplets began their breakup within a distance interval from  $0.02c$  to  $0.09c$  where  $c$  is the chord of the airfoil. For the large airfoil (chord = 0.710 m), the distance at which the droplets begin their breakup, non-dimensionalized against the chord of the airfoil, was plotted against the diameter of the droplets for velocities of 70 and 90 m/sec (Fig. 23). There is scatter in the data but the results indicate that as the velocity is increased the droplets begin their breakup process further away from the leading edge of the airfoil.

The results of the work presented here will help in the development of improved break-up models for ice accretion codes. The results also indicate the need for better understanding of the break-up process and the distance from the airfoil at which it occurs.

## Conclusions

A subset of the data from the 2011 droplet breakup experiment conducted in the rotating rig test cell at the Instituto Nacional de Técnica Aeroespacial (INTA) in Madrid, Spain, was analyzed. The diameter of the droplets analyzed ranged from 500 to 1800  $\mu\text{m}$ . Three airfoils were tested with the data presented being mostly for the larger airfoil with a chord of 0.710 m. The airfoil velocities tested were 50, 60, 70, 80, and 90 m/sec. Most of the data presented is for the 90 m/sec cases. From the analysis of the data the following conclusions can be stated about the results:

- Droplet deformation and breakup follows a well defined pattern with some modifications for the small droplets (diameters close to 100  $\mu\text{m}$ ) and very large droplets (diameters larger than 1500  $\mu\text{m}$ ). The droplet is initially spherical and as the slip velocity increases it deforms into an oblate spheroid, symmetric with respect to the horizontal axis, asymmetric with respect to the vertical axis and rotationally symmetric with respect to the axis in the direction of motion of the droplet, in a frame of reference at rest with respect to the airfoil. During this part of the deformation the width of the droplet decreases and its height increases as the droplet becomes elongated while maintaining the oblate spheroid shape. The width reaches a minimum value where the deformation ends and the actual breakup begins. At this point the droplet changes from the elongated oblate spheroid with a rear bulge to a front bulge or protuberance with a shape resembling a “hat” that grows initially and then starts to lose mass by shearing. The mass loss by shearing continues around the droplet core and forms a tail behind the droplet followed by a cloud of small droplets. The very large droplets fall oscillating heavily and the oscillation and large inertia delay the onset of the typical deformation pattern although it is still there.
- Images of the final stages of droplet breakup showed a cloud of water behind the core-tail of the original droplet as mass is lost through shearing. This indicates that at least some of the mass of the droplet ends up in a cloud of small droplets that may be carried away by the flow depending on their sizes and how far they are from the leading edge.
- The width of the droplet, as measured with a data analysis digital image processing program, decreases as the droplet approaches the airfoil and reaches a minimum value at the initiation of the droplet breakup where it begins to increase.
- The diameter of the droplets, based on the volume of the oblate spheroid, remained constant until the initiation of breakup providing additional evidence that the spheroid is rotationally symmetric around the axis pointing in the direction of the motion of the droplet with respect to the airfoil.
- The exponential decrease of the air velocity generates the slip velocity of the droplet and propagates to the behavior of the other parameters against time. Consequently the droplet horizontal displacement, velocity, acceleration, slip velocity, Weber number, Reynolds number, Bond number and drag coefficient all display exponential behavior against time.
- Uncertainties in the data result from the resolution of the imaging system, the curve fitting involved in the calculation of the velocity and acceleration and the method used to choose the threshold value for the conversion of the images from grayscale to binary prior to segmentation and tracking of a droplet.



Uncertainties also come from the deviation of the droplet geometry from that of an oblate spheroid. The error from the resolution affects the measurement of the diameter of the droplets. The error from the curve fitting affects the calculation of the velocity acceleration and slip velocity. The threshold error affects the measurement of the diameter

- Droplet deformation was defined as the ratio of the major and minor axis of an ellipse superimposed on the deforming droplet. Droplet deformation was studied for a sample of nineteen droplets with a range of diameters from 500 to 1800  $\mu\text{m}$ . For individual droplets, deformation was found to increase exponentially against time and nearly linearly against the Weber and Reynolds numbers. Against acceleration, the rate of change increased rapidly initially and then settled to an almost linear behavior.
- The data used to study the behavior of the deformation against droplet diameter at constant slip velocities showed scattering that increased as the slip velocity increased. Although some scattering was anticipated since droplets of different diameters at same slip velocity have different Weber and Reynolds numbers, scattering was also present in droplets with closer diameter values. The scattering was due to the difference in individual acceleration of each droplet and possibly other intrinsic parameters to the droplet. As measured by the standard deviation of the samples, scattering could be decreased by plotting of the deformation scaled with the Bond number against the diameter of the droplets at same slip velocity.
- The drag coefficient was found to increase linearly with deformation as the droplet deformed from a sphere to an oblate spheroid before the beginning of the actual breakup. The drag coefficient also increased linearly with the Reynolds number.
- Data for the distance at which droplets breakup for different velocities and two airfoils showed high scattering but it was found that all droplets breakup within a distance interval of  $0.02c$  to  $0.09c$ . For the large airfoil (chord =  $0.710$ ) at an airfoil velocity of  $90$  m/sec the droplets broke up earlier (further away from the leading edge) than at a velocity of  $70$  m/sec.
- Study of the deformation of individual droplets was possible and the overall behavior of the droplets was similar. Comparison between different droplets was very difficult because droplet deformation depends on several parameters: Weber number, Reynolds number, Bond number and possibly additional parameters intrinsic to the droplets. Varying one parameter at a time was not possible and no parameter was found to be more dominant with respect to the droplet deformation than the others.

The results of the work presented here will help in the development of improved break-up models for ice accretion codes. The results also indicate the need for better understanding of the break-up process and the distance from the airfoil at which it occurs.

## References

1. Vargas, M. and Feo, A., "Experimental Observations on the Deformation and Breakup of Water Droplets near the Leading Edge of an Airfoil," NASA/TM—2011-216946, AIAA Paper 2010-7670, August 2010.
2. Feo, A., Vargas, M., and Sor, S., "Rotating Rig Development for Droplet Deformation/Breakup and Impact Induced by Aerodynamic Surfaces," SAE Technical Paper 2011-38-0087, 2011, doi:10.4271/2011-38-0087.
3. Vargas, M., "NASA Glenn Matlab Computer Program for the Analysis of Droplet Deformation and Breakup," (to be published).
4. Sor, S., García-Magariño, A., "Diameter and Axisymmetry Measurements of a Water Droplet Impinging on an Airfoil," INTA Document No. AE-1NO-4420-065, March 2012.
5. Sor, S., Personal communication on PIV data obtained at the INTA's Rotating Rig Facility
6. Otsu, N., "A Threshold Selection Method From Gray-Level Histograms," IEEE Transactions on Systems, Man, and Cybernetics, Vol. 9, No. 1, pp. 62-66, 1979.

TABLE 1.—DBKUP AIRFOIL COORDINATES

X-Coordinate	Y-Coordinate	X-Coordinate	Y-Coordinate
1.0000	0.0000	0.0000	0.0000
0.9989	-0.0009	0.0011	0.0139
0.9957	-0.0014	0.0043	0.0310
0.9904	-0.0025	0.0096	0.0498
0.9830	-0.0042	0.0170	0.0674
0.9735	-0.0064	0.0265	0.0842
0.9619	-0.0089	0.0381	0.1007
0.9484	-0.0120	0.0516	0.1170
0.9330	-0.0155	0.0670	0.1318
0.9157	-0.0195	0.0843	0.1458
0.8967	-0.0240	0.1033	0.1584
0.8759	-0.0291	0.1241	0.1700
0.8536	-0.0347	0.1465	0.1797
0.8297	-0.0410	0.1703	0.1880
0.8044	-0.0479	0.1956	0.1943
0.7778	-0.0554	0.2222	0.1985
0.7500	-0.0634	0.2500	0.2007
0.7211	-0.0721	0.2789	0.2006
0.6913	-0.0815	0.3087	0.1985
0.6607	-0.0915	0.3393	0.1938
0.6294	-0.1019	0.3706	0.1870
0.5976	-0.1128	0.4025	0.1780
0.5653	-0.1240	0.4347	0.1683
0.5327	-0.1353	0.4673	0.1577
0.5000	-0.1466	0.5000	0.1466
0.4673	-0.1577	0.5327	0.1353
0.4347	-0.1683	0.5653	0.1240
0.4025	-0.1780	0.5976	0.1128
0.3706	-0.1870	0.6294	0.1019
0.3393	-0.1938	0.6607	0.0915
0.3087	-0.1985	0.6913	0.0815
0.2789	-0.2006	0.7211	0.0721
0.2500	-0.2007	0.7500	0.0634
0.2222	-0.1985	0.7778	0.0554
0.1956	-0.1943	0.8044	0.0479
0.1703	-0.1880	0.8297	0.0410
0.1465	-0.1797	0.8536	0.0347
0.1241	-0.1700	0.8759	0.0291
0.1033	-0.1584	0.8967	0.0240
0.0843	-0.1458	0.9157	0.0195
0.0670	-0.1318	0.9330	0.0155
0.0516	-0.1170	0.9484	0.0120
0.0381	-0.1007	0.9619	0.0089
0.0265	-0.0842	0.9735	0.0064
0.0170	-0.0674	0.9830	0.0042
0.0096	-0.0498	0.9904	0.0025
0.0043	-0.0310	0.9957	0.0014
0.0011	-0.0139	0.9989	0.0009
0.0000	0.0000	1.0000	0.0000

TABLE 2.—TEST CONDITIONS FOR DROPLETS ANALYZED  
 [Airfoil DBKUP 001—Chord size 0.710 m.]

Run number	Orifice, $\mu\text{m}$	Droplet theoretical diameter, $\mu\text{m}$	Airfoil model velocity, m/sec	Magnification	Resolution H x V pixels/pixels per mm	Frame rate Frames/sec
072011.11	200	400	80	1/1	192×312/14.26	75,000
072011.13A	200	400	90	1/1	192×312/14.26	75,000
072011.13B	200	400	90	1/1	192×312/14.26	75,000
072011.14B	200	400	90	1/1	192×312/14.26	75,000
072011.14C	200	400	90	1/1	192×312/14.26	75,000
072111.05	100	200	90	1/1	192×312/14.26	75,000
072611.15A	700	1400	90	1/1	192×312/14.26	75,000
072611.15B	700	1400	90	1/1	192×312/14.26	75,000
072611.16	500	1000	90	1/1	192×312/14.26	75,000
072611.18	400	800	90	1/1	256×312/14.26	75,000

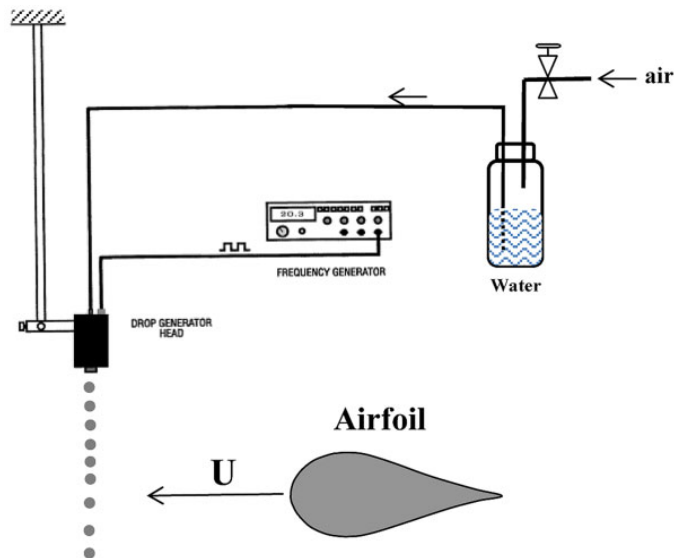


Figure 1.—Conceptual view of the experiment.

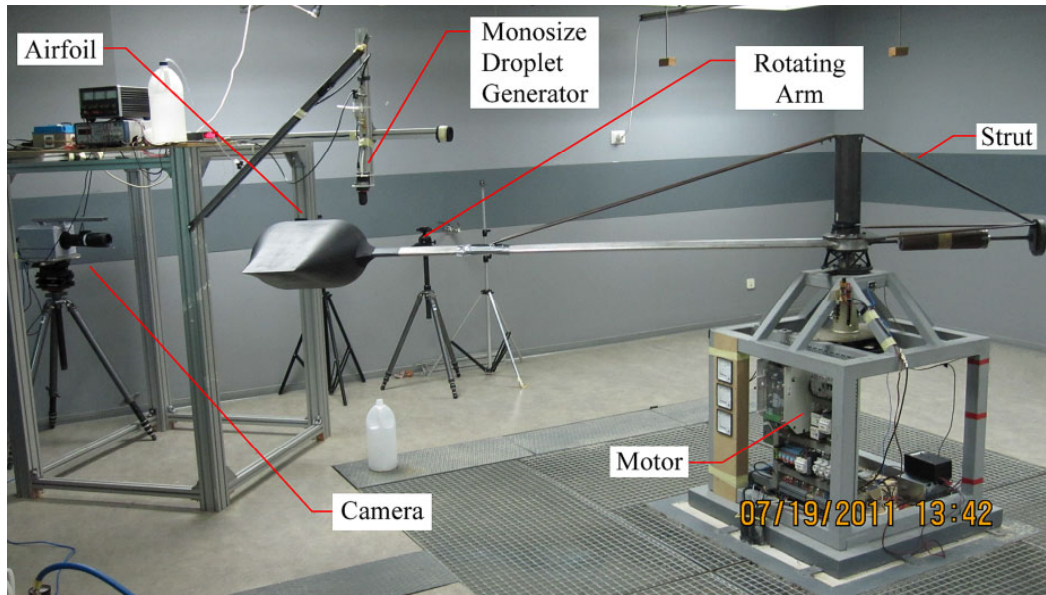


Figure 2.—Experiment set-up in the INTA test cell.



Figure 3.—Close-up picture of airfoil (DBKUP 003, chord = 0.710 m), TSI droplet generator and the high speed camera.

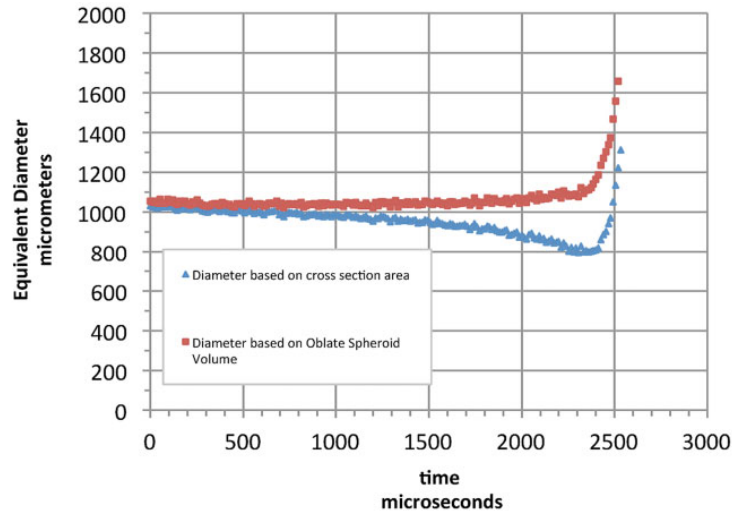
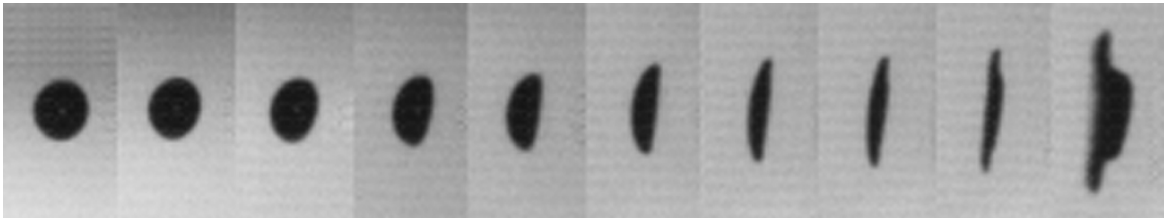


Figure 4.—Equivalent Diameter against time. Run 072011.14C droplet #1, droplet diameter = 1062  $\mu\text{m}$ , airfoil chord = 0.710 m, airfoil velocity = 90 m/sec. The red data (rectangles) correspond to the diameter based on the volume of the asymmetric oblate spheroid. The blue data (triangles) correspond to the diameter based on the circular area of the droplet cross section. In the calculations made for this paper only the diameter based on the volume of the asymmetric oblate spheroid was used.



	(a)	(b)	(c)	(d)	(e)	(f)	(g)	(h)	(i)	(j)
Frame #	20	60	100	140	160	180	190	194	200	210
Time, $\mu\text{sec}$	253	787	1320	1853	2120	2387	2520	2573	2653	2787
x-distance from airfoil, mm	225	177	129	82	58	34	23	18	11	0
Vslip, m/sec	15.5	19.8	25.9	35.4	42.9	54.0	61.8	65.3	71.3	82.6
We	4.21	6.90	11.77	21.99	32.20	51.36	67.05	75.07	89.42	119.95
Re	1120	1433	1872	2559	3102	3911	4469	4728	5161	5977
Bo	2.14	2.50	3.20	8.10	21.55	71.34	134.75	174.41	257.47	495.06
Cd	0.68	0.48	0.36	0.49	0.89	1.85	2.75	3.10	3.84	5.50

Figure 5.—Sequence of deformation and initiation of breakup. Run 072011.14C droplet #1, droplet diameter = 1062  $\mu\text{m}$ , airfoil chord = 0.710 m, airfoil velocity = 90 m/sec. The sequence shows the corresponding values for several of the parameters at each stage of the droplet deformation.

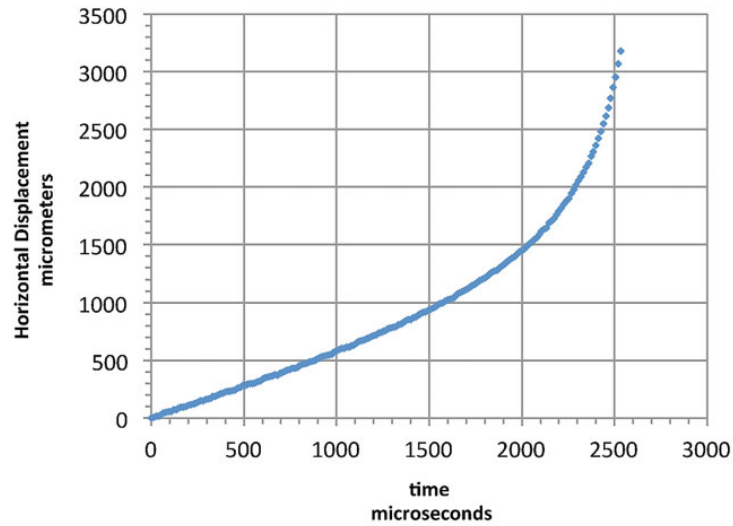


Figure 6.—Horizontal Displacement against time. Run 072011.14C droplet #1, droplet diameter = 1062  $\mu\text{m}$ , airfoil chord = 0.710 m, airfoil velocity = 90 m/sec.

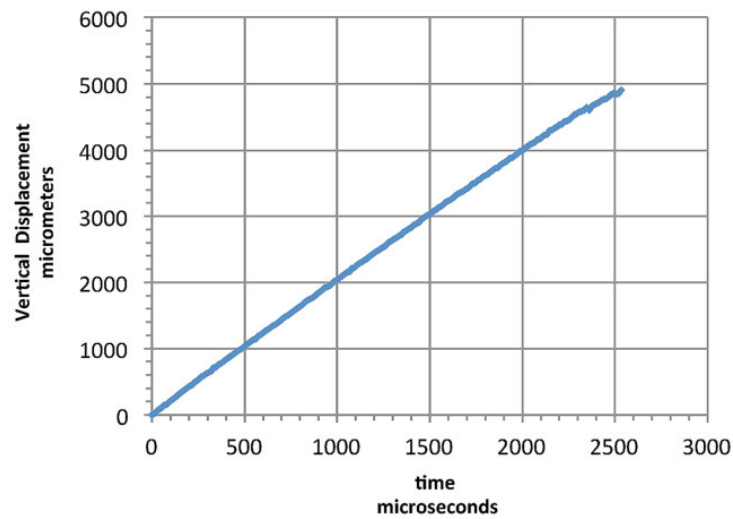


Figure 7.—Vertical Displacement against time. Run 072011.14C droplet #1, droplet diameter = 1062  $\mu\text{m}$ , airfoil chord = 0.710 m, airfoil velocity = 90 m/sec.

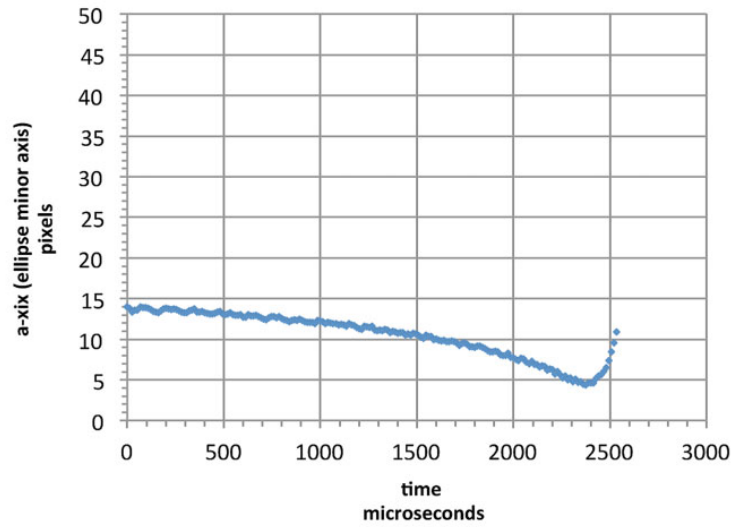


Figure 8.—Minor axis of ellipse superimposed on deformed droplet against time. Run 072011.14C droplet #1, droplet diameter = 1062  $\mu\text{m}$ , airfoil chord = 0.710 m, airfoil velocity = 90 m/sec.

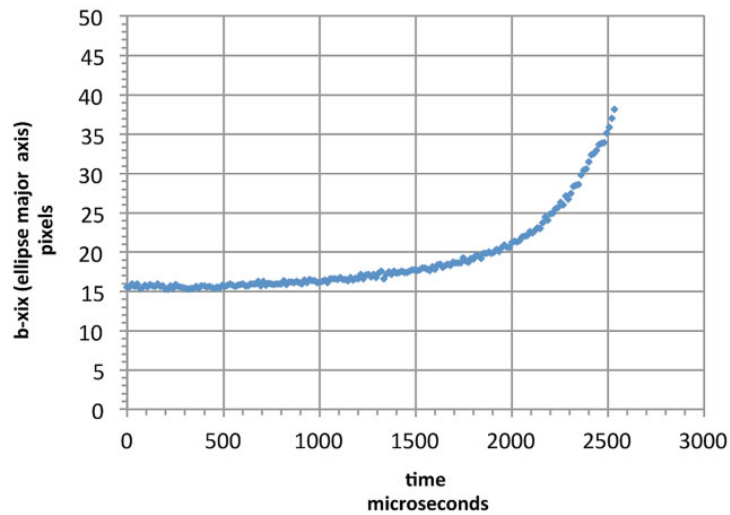


Figure 9.—Major axis of ellipse superimposed on deformed droplet against time. Run 072011.14C droplet #1, droplet diameter = 1062  $\mu\text{m}$ , airfoil chord = 0.710 m, airfoil velocity = 90 m/sec.

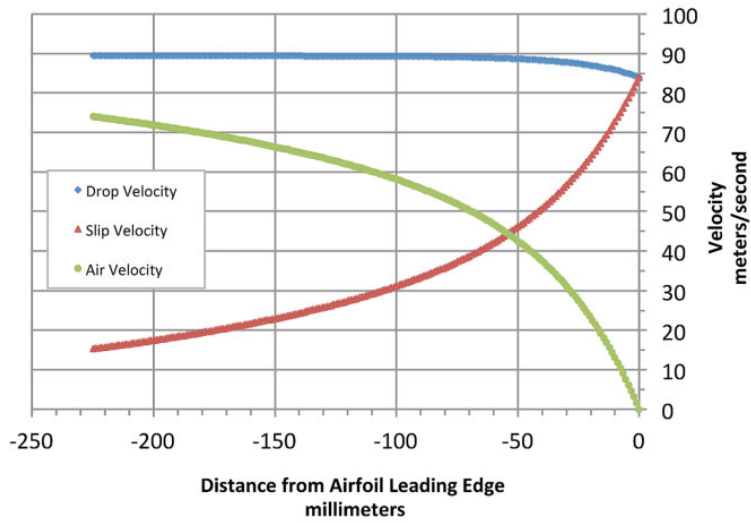


Figure 10.—Drop velocity, air velocity and slip velocity against the distance from the airfoil leading edge along the stagnation line. Run 072011.14C droplet #1, droplet diameter = 1062  $\mu\text{m}$ , airfoil chord = 0.710 m, airfoil velocity = 90 m/sec.

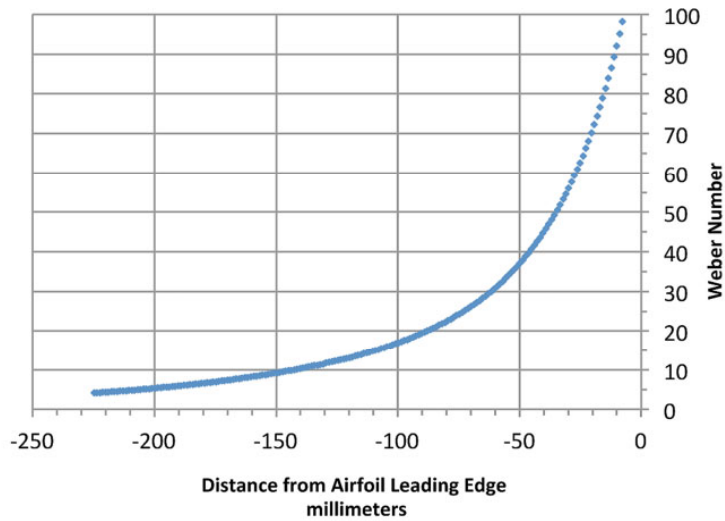


Figure 11.—Weber number against the distance from the leading edge of the airfoil along the stagnation line. Run 072011.14C droplet #1, droplet diameter = 1062  $\mu\text{m}$ , airfoil chord = 0.710 m, airfoil velocity = 90 m/sec.



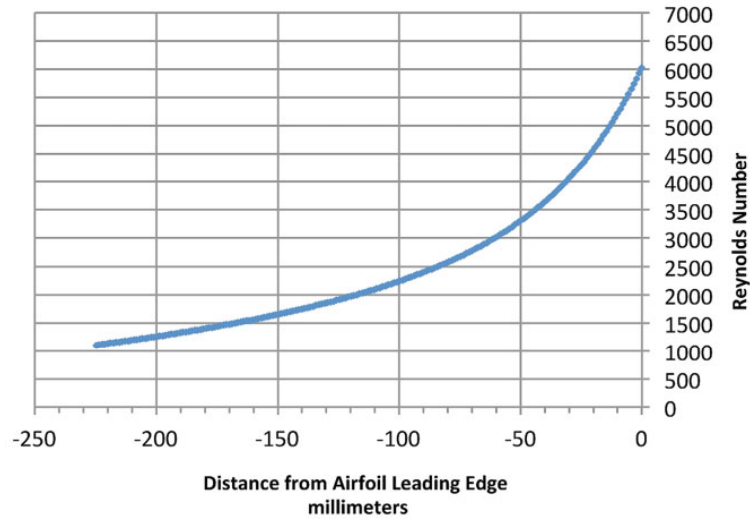


Figure 12.—Reynolds number against the distance from the leading edge of the airfoil along the stagnation line. Run 072011.14C droplet #1, droplet diameter = 1062  $\mu\text{m}$ , airfoil chord = 0.710 m, airfoil velocity = 90 m/sec.

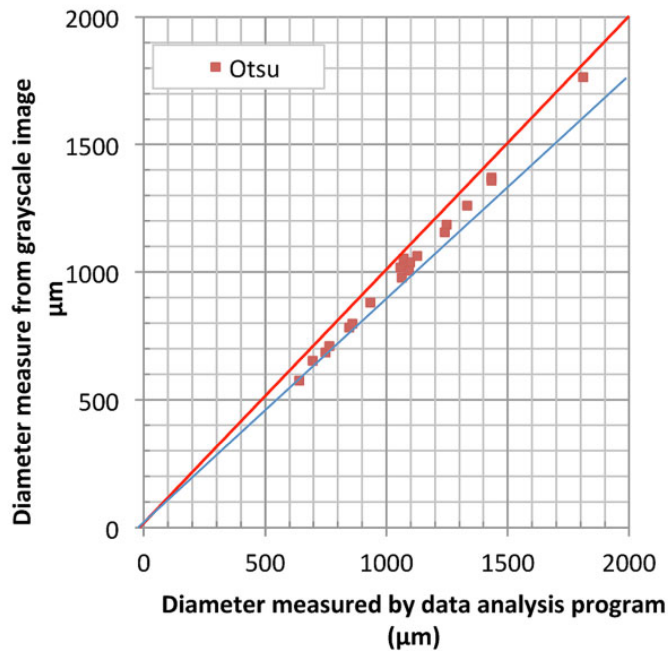


Figure 13.—Diameter of tracked droplet. Measurement of droplet diameter made manually from the grayscale image in the first tracking frame for nineteen drop tracking cases is plotted against the diameter of the same droplet measured with the digital image processing data analysis program after converting the image to binary using Otsu's thresholding methodology.

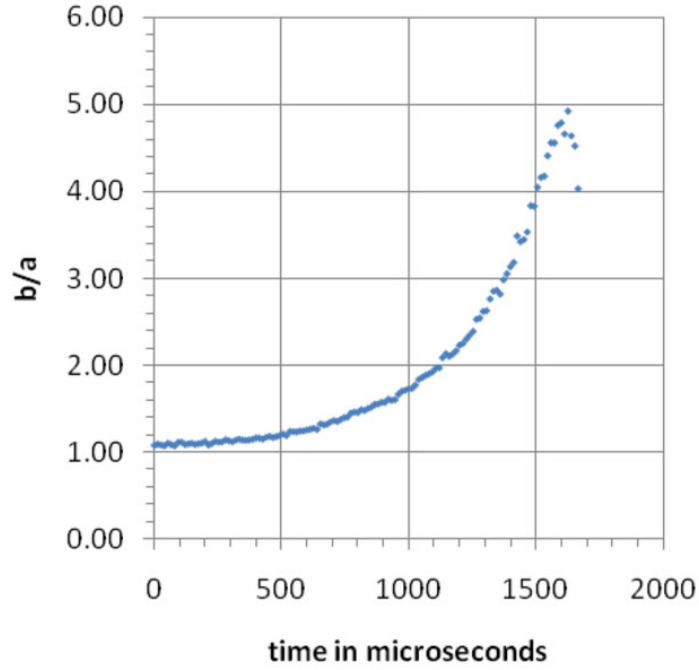


Figure 14.—Droplet deformation against time. Run 072611.15B.9 droplet #2, droplet diameter = 1431  $\mu\text{m}$ , airfoil chord = 0.710 m, airfoil velocity = 90 m/sec.

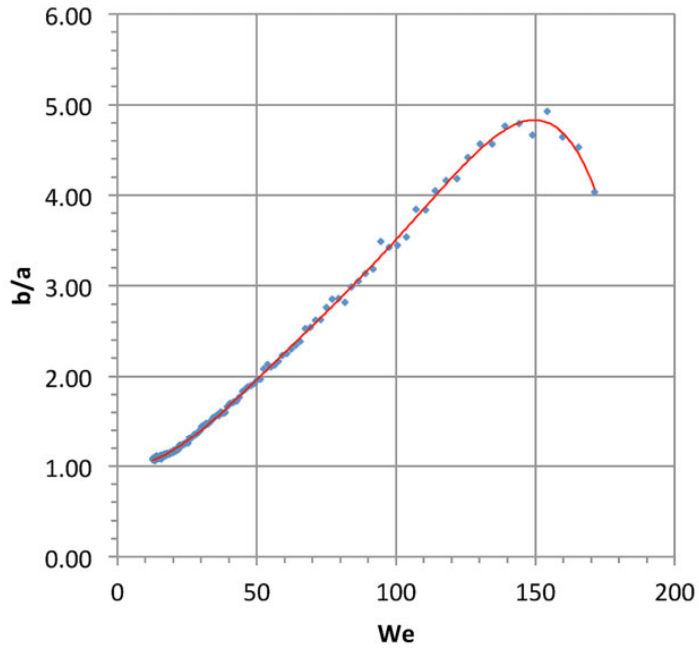


Figure 15.—Droplet deformation against Weber number. Run 072611.15B.9 droplet #2, droplet diameter = 1431  $\mu\text{m}$ , airfoil chord = 0.710 m, airfoil velocity = 90 m/sec.

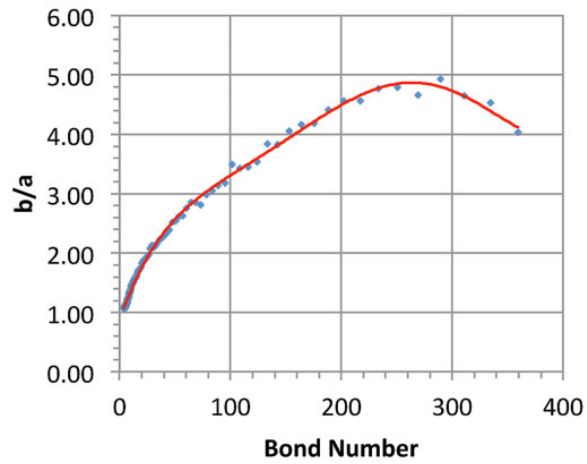


Figure 16.—Droplet deformation against Bond Number.  
 Run 072611.15B.9 droplet #2, droplet diameter =  
 1431  $\mu\text{m}$ , airfoil chord = 0.710 m, airfoil velocity =  
 90 m/sec.

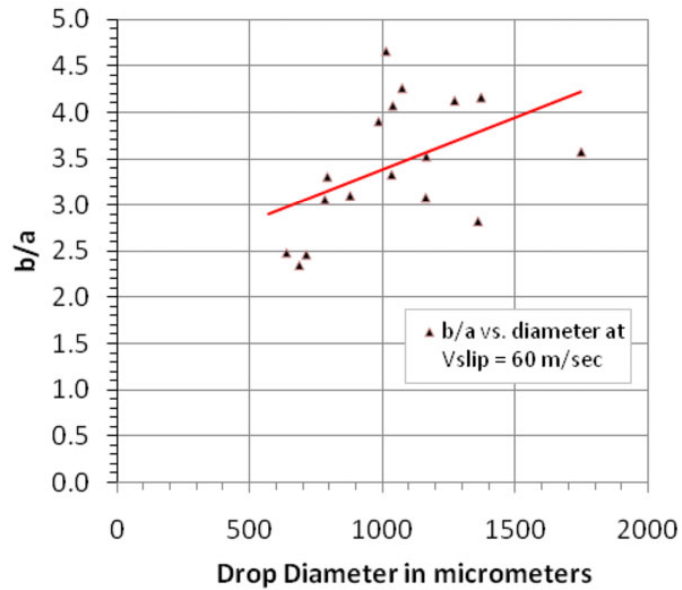


Figure 17.—Droplet deformation against droplet diameter, at  
 constant slip velocity of 60 m/sec, airfoil chord = 0.710 m,  
 airfoil velocity = 90 m/sec.

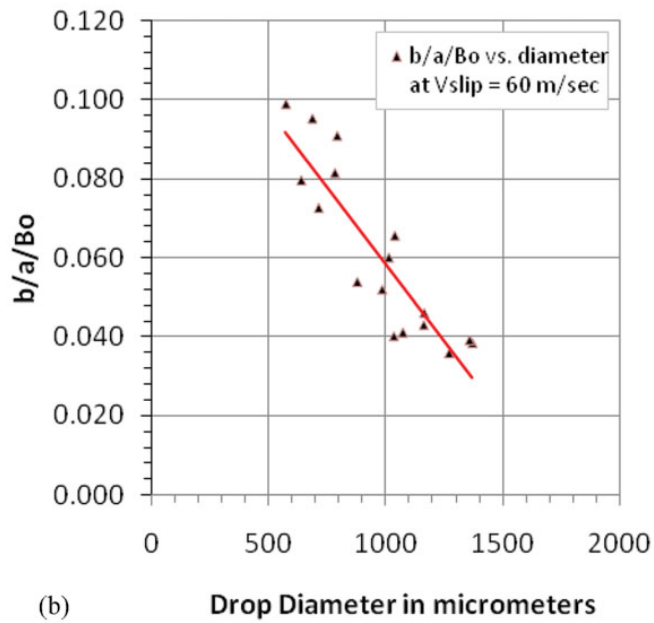
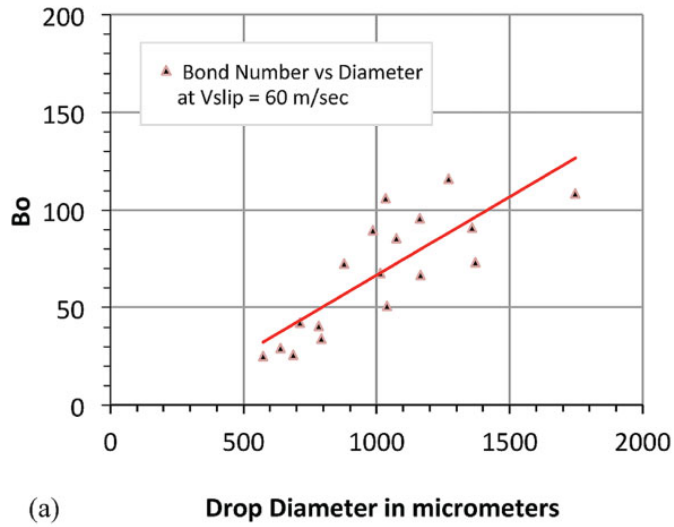


Figure 18.—(a) Bond number against droplet diameter at constant slip velocity of 60 m/sec; (b) The deformation/Bond Number. Both plots for an airfoil chord = 0.710 m, airfoil velocity = 90 m/sec.

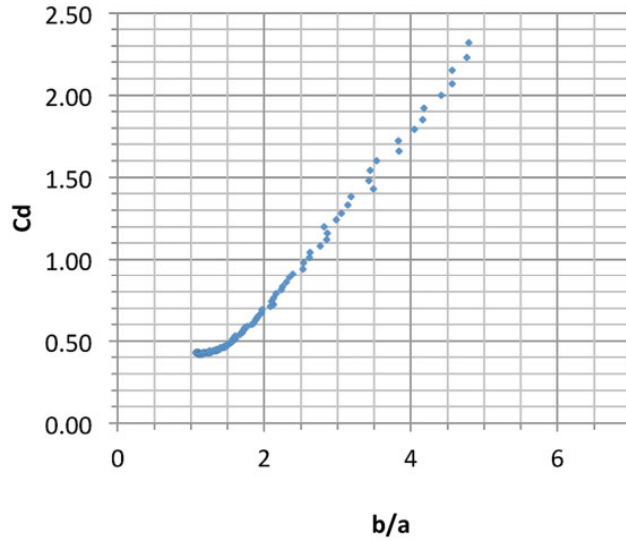


Figure 19.—Drag coefficient against deformation. Run 072011.14C droplet #1, droplet diameter = 1062  $\mu\text{m}$ , airfoil chord = 0.710 m, airfoil velocity = 90 m/sec.

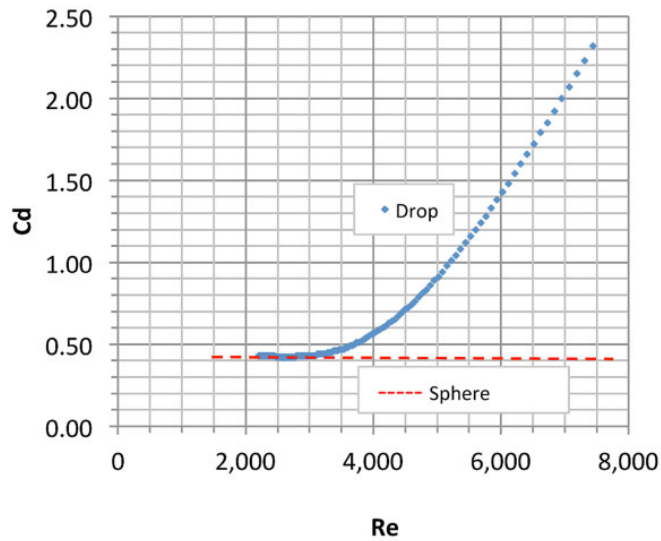
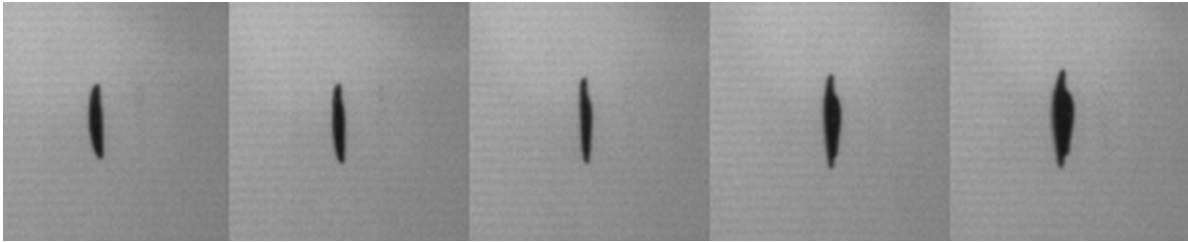
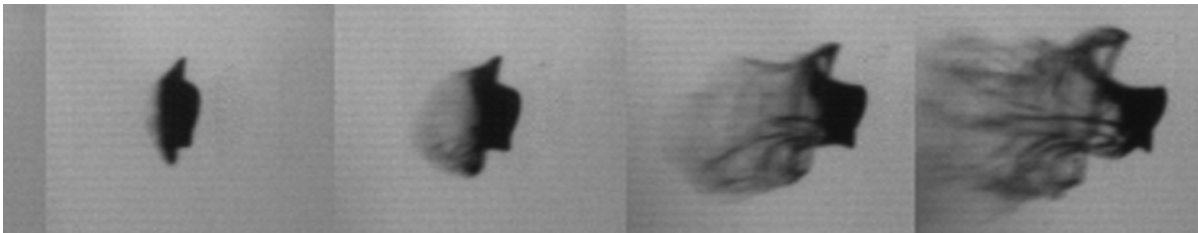


Figure 20.—Drag coefficient for the droplet against Reynolds number. For comparison, the drag coefficient for a solid sphere is plotted for the same range of Reynolds number. Run 072011.14C droplet #1, droplet diameter = 1062  $\mu\text{m}$ , airfoil chord = 0.710 m, airfoil velocity = 90 m/sec.



	(a)	(b)	(c)	(d)	(e)
Frame #	190	194	198	203	205
Time (μsec)	2520	2573	2627	2653	2720
x-distance from Airfoil (mm)	32	28	23	17	15



	(f)	(g)	(h)	(i)	(j)
Frame #	207	209	212	215	218
Time (μsec)	2747	2773	2813	2853	2893
x-distance from Airfoil (mm)	13	11	8	5	2

Figure 21.—Sequence of deformation and breakup. Run 072011.14B.1 droplet #1, droplet diameter = 1032 μm, airfoil chord = 0.710 m, airfoil velocity = 90 m/sec. Several parameters are shown for each stage in the droplet deformation.

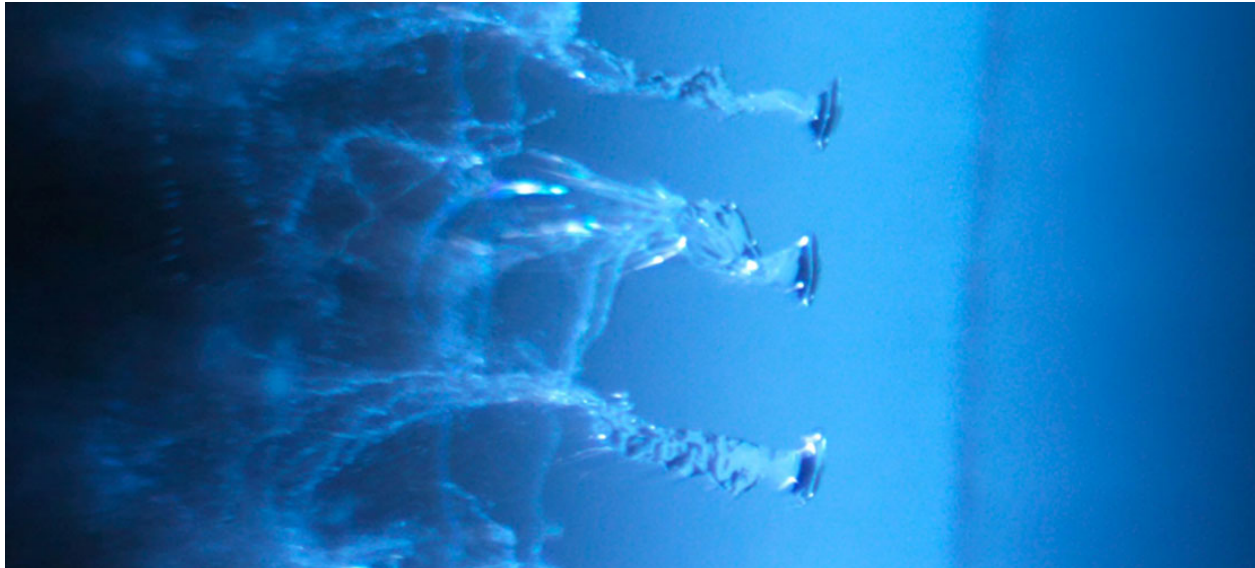


Figure 22.—Final stage of breakup for a droplet as it approaches the airfoil. The core of the droplet is followed by a tail of water that ends up in a cloud of smaller droplets. The sequence illustrates the shearing process that eventually consumes the droplet.

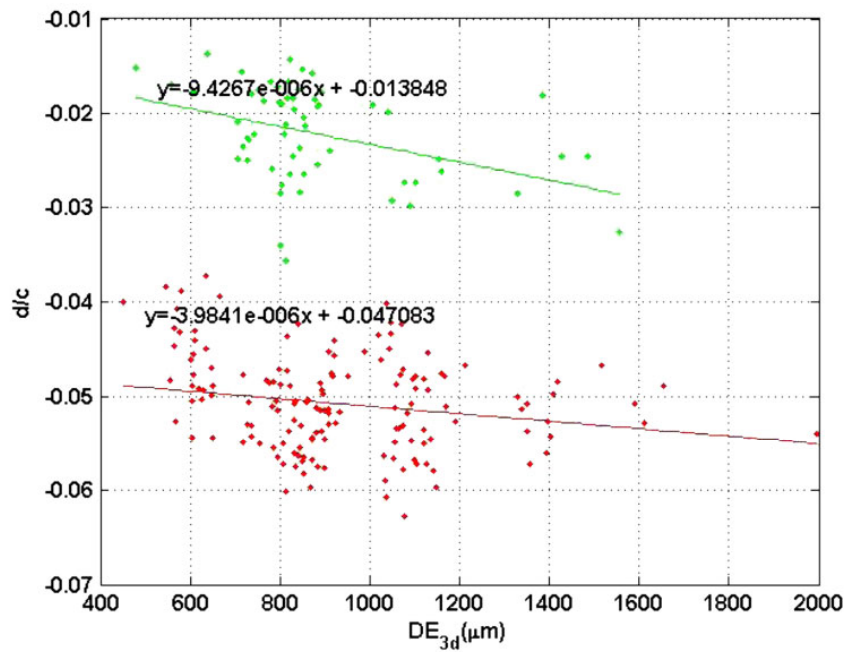


Figure 23.—Distance that a droplet begins to breakup divided by the chord of the airfoil versus the diameter of the droplet for the airfoil with chord = 0.710 m at two airfoil velocities: 70 m/sec (green data points) and 90 m/sec (red data points).

REPORT DOCUMENTATION PAGE			Form Approved OMB No. 0704-0188		
<p>The public reporting burden for this collection of information is estimated to average 1 hour per response, including the time for reviewing instructions, searching existing data sources, gathering and maintaining the data needed, and completing and reviewing the collection of information. Send comments regarding this burden estimate or any other aspect of this collection of information, including suggestions for reducing this burden, to Department of Defense, Washington Headquarters Services, Directorate for Information Operations and Reports (0704-0188), 1215 Jefferson Davis Highway, Suite 1204, Arlington, VA 22202-4302. Respondents should be aware that notwithstanding any other provision of law, no person shall be subject to any penalty for failing to comply with a collection of information if it does not display a currently valid OMB control number.</p> <p>PLEASE DO NOT RETURN YOUR FORM TO THE ABOVE ADDRESS.</p>					
1. REPORT DATE (DD-MM-YYYY) 01-09-2012		2. REPORT TYPE Technical Memorandum		3. DATES COVERED (From - To)	
4. TITLE AND SUBTITLE Mechanism of Water Droplet Breakup Near the Leading Edge of an Airfoil			5a. CONTRACT NUMBER		
			5b. GRANT NUMBER		
			5c. PROGRAM ELEMENT NUMBER		
6. AUTHOR(S) Vargas, Mario; Sor, Suthyvann; Magarino, Adelaida, Garcia			5d. PROJECT NUMBER		
			5e. TASK NUMBER		
			5f. WORK UNIT NUMBER WBS 648987.02.02.03.10		
7. PERFORMING ORGANIZATION NAME(S) AND ADDRESS(ES) National Aeronautics and Space Administration John H. Glenn Research Center at Lewis Field Cleveland, Ohio 44135-3191			8. PERFORMING ORGANIZATION REPORT NUMBER E-18391		
9. SPONSORING/MONITORING AGENCY NAME(S) AND ADDRESS(ES) National Aeronautics and Space Administration Washington, DC 20546-0001			10. SPONSORING/MONITOR'S ACRONYM(S) NASA		
			11. SPONSORING/MONITORING REPORT NUMBER NASA/TM-2012-217704		
12. DISTRIBUTION/AVAILABILITY STATEMENT Unclassified-Unlimited Subject Category: 03 Available electronically at <a href="http://www.sti.nasa.gov">http://www.sti.nasa.gov</a> This publication is available from the NASA Center for AeroSpace Information, 443-757-5802					
13. SUPPLEMENTARY NOTES					
14. ABSTRACT This work presents results of an experimental study on droplet deformation and breakup near the leading edge of an airfoil. The experiment was conducted in the rotating rig test cell at the Instituto Nacional de Tecnica Aeroespacial (INTA) in Madrid, Spain. The airfoil model was placed at the end of the rotating arm and a monosize droplet generator produced droplets that fell from above, perpendicular to the path of the airfoil. The interaction between the droplets and the airfoil was captured with high speed imaging and allowed observation of droplet deformation and breakup as the droplet approached the airfoil near the stagnation line. Image processing software was used to measure the position of the droplet centroid, equivalent diameter, perimeter, area, and the major and minor axes of an ellipse superimposed over the deforming droplet. The horizontal and vertical displacement of each droplet against time was also measured, and the velocity, acceleration, Weber number, Bond number, Reynolds number, and the drag coefficients were calculated along the path of the droplet to the beginning of breakup. Droplet deformation is defined and studied against main parameters. The high speed imaging allowed observation of the actual mechanism of breakup and identification of the sequence of configurations from the initiation of the breakup to the disintegration of the droplet. Results and comparisons are presented for droplets of diameters in the range of 500 to 1800 µm, and airfoil velocities of 70 and 90 m/sec.					
15. SUBJECT TERMS Icing; Engine icing					
16. SECURITY CLASSIFICATION OF:			17. LIMITATION OF ABSTRACT  UU	18. NUMBER OF PAGES  34	19a. NAME OF RESPONSIBLE PERSON STI Help Desk (email: <a href="mailto:help@sti.nasa.gov">help@sti.nasa.gov</a> )
a. REPORT U	b. ABSTRACT U	c. THIS PAGE U			19b. TELEPHONE NUMBER (include area code) 443-757-5802





